

Robophysical modeling of spacetime dynamics

Shengkai Li,¹ Hussain N. Gynai,² Steven Tarr,¹ Pablo Laguna,³ Gongjie Li,¹ and Daniel I. Goldman¹

¹*School of Physics, Georgia Institute of Technology, Atlanta, Georgia 30332, USA*

²*School of Mathematics, Georgia Institute of Technology, Atlanta, Georgia 30332, USA*

³*Center for Gravitational Physics, Department of Physics, University of Texas at Austin, Austin, Texas 78712, USA*

(Dated: February 11, 2022)

Systems consisting of spheres rolling on elastic membranes have been used as educational tools to introduce a core conceptual idea of General Relativity (GR): how curvature guides the movement of matter. However, previous studies have revealed that such schemes cannot accurately represent relativistic dynamics in the laboratory. Dissipative forces cause the initially GR-like dynamics to be transient and consequently restrict experimental study to only the beginnings of trajectories; dominance of Earth’s gravity forbids the difference between spatial and temporal spacetime curvatures. Here by developing a mapping between dynamics of a wheeled vehicle on a spandex membrane, we demonstrate that an active object that can prescribe its speed can not only obtain steady-state orbits, but also use the additional parameters such as speed to tune the orbits towards relativistic dynamics. Our mapping demonstrates how activity mixes space and time in a metric, shows how active particles do not necessarily follow geodesics in the real space but instead follow geodesics in a fiducial spacetime. The mapping further reveals how parameters such as the membrane elasticity and instantaneous speed allow programming a desired spacetime such as the Schwarzschild metric near a non-rotating black hole. Our mapping and framework point the way to the possibility to create a robophysical analog gravity system in the laboratory at low cost and provide insights into active matter in deformable environments and robot exploration in complex landscapes.

Introduction. Systems consisting of spheres rolling on curved surfaces [1, 2] are a well known non-hydrodynamic analog to gravity. In such readily accessible systems, researchers have made intriguing connections to gravity such as Kepler-like laws, precession, and the stability of orbits. However, their studies have also found that these systems do not exactly mimic astrophysical gravity. For instance, the scaling between the period and radius is $T \propto r^{2/3}$ [3] instead of the $T \propto r^{3/2}$ in Kepler’s law. Additionally, the sphere on the elastic is passive; as a result, not only do trajectories decay quickly, but also the tunable parameters are limited to only the boundary conditions and the mass of the marble.

We hypothesized that making the object “active” – an internally driven robot – would allow mechanical systems to better model GR in part because of the ability to study long time steady states. We further reasoned that the programmability and sensory capabilities of increasingly low-cost and powerful “robophysical” models [4, 5] could allow tuning of parameters that lead to inexact mimics of GR in passive systems. Indeed, our recent work [6] built a framework to understand how the field-mediated dynamics of active agents on flexible membranes demonstrate in the words of Wheeler’s famous aphorism: “matter tells spacetime how to curve and spacetime tells matter how to move” [7]. In particular, we show that the spacetime followed by an active object can be tuned by varying system parameters such as the membrane elasticity and the speed of the object.

Here we amplify on and extend the scheme introduced in [6] and demonstrate how the activity can lead to an exact mapping to GR. We first show how an active

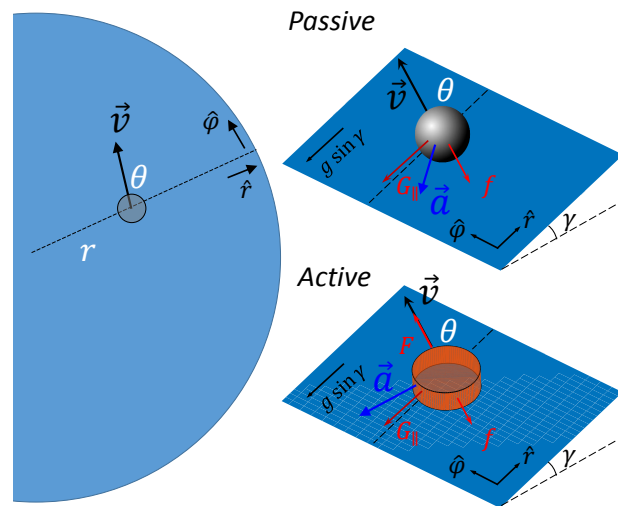


FIG. 1. **A passive object versus an active object on a membrane.** While a passive marble is only subjected to friction and Earth’s gravity that leads to energy dissipation as $\vec{F} \cdot \vec{v} \propto \vec{a} \cdot \vec{v} < 0$, an active object with an additional drive force can keep steady-state motion with prescribed speed as $\vec{a} \cdot \vec{v} = 0$.

object with prescribed speed on an elastic membrane produces longer and more controllable trajectories compared with a passive marble. We then deduce the spacetime it follows, and subsequently show one can program the spacetime with a Schwarzschild orbit as an example. We posit that a future robot car controlled in the way we describe could mechanically mimic black

holes dynamics in the laboratory, at low cost and with strong pedagogical value.

An active object with fixed speed on an elastic membrane. We first consider an active object prescribed with a constant speed on a circular elastic membrane. Later, we will discuss the general case of time-varying speed. To prevent the object from simply following a near-straight-line spatial geodesic with a spatial curvature

$$ds^2 = \Psi^2 dr^2 + r^2 d\varphi^2 \quad (1)$$

where $\Psi^2 = 1 + z'^2$ and prime denotes the derivative with respect to r , we want the object to turn according to the instantaneous local curvature. To do so, we propel a vehicle with a differential drive that drives the center of mass of the vehicle with a prescribed speed while the speed difference between the two wheels depends on the local slope.

We first compare the trajectories of the active vehicle with those of a passive marble having the same mass as the vehicle. We released them with the same velocity on the same membrane individually. The speeds of the vehicle and marble are set by adjusting the voltage on the motor and the releasing height on the guiding track (Fig.2a) respectively. The trajectories collected from experiments showed that the active vehicle produced trajectories much more persistent (Fig.2c) than the passive marble which barely finished the first revolution (Fig.2b).

To understand these orbits, we follow the models in [6, 8]. While a passive marble dissipates energy as $\vec{a} \cdot \vec{v} < 0$ (Fig. 1), an active object can conserve its speed when the driving force dynamically balances with the friction and exactly makes $\vec{a} \cdot \vec{v} = 0$ (Fig.3a). Therefore, the acceleration for a constant-speed motion can be written as

$$\frac{a_\varphi}{r} = \ddot{\varphi} + \frac{2\dot{r}\dot{\varphi}}{r} = \frac{a}{r} \cos \theta \quad (2)$$

$$a_r = \ddot{r} - \frac{r\dot{\varphi}^2}{\Psi^2} + \frac{\Psi'}{\Psi}\dot{r}^2 = -\frac{a}{\Psi} \sin \theta. \quad (3)$$

where θ is the heading angle between the radial direction and the velocity on an isotropic circular membrane.

Though the speed is constant, the change of the velocity (the scalar acceleration a) depends on the local slope γ (Fig.1). Since γ varies with radius (position) r , a is also a function of r . Additionally, a should also depend on velocity in general. However, given that the velocity has constant magnitude as the speed is constant, this dependence is reduced to one degree of freedom. For our convenience, we chose the direction of the velocity, θ . If we consider an active object without chiral bias such that its trajectory has a mirror symmetry, the dependence of a (thus a_φ) on θ should be anti-symmetric about $\theta = 0$, as otherwise the clockwise ($\theta(t=0) = \theta_0$) and counter-clockwise ($\theta(t=0) = -\theta_0$) trajectories (Fig.3b) will not

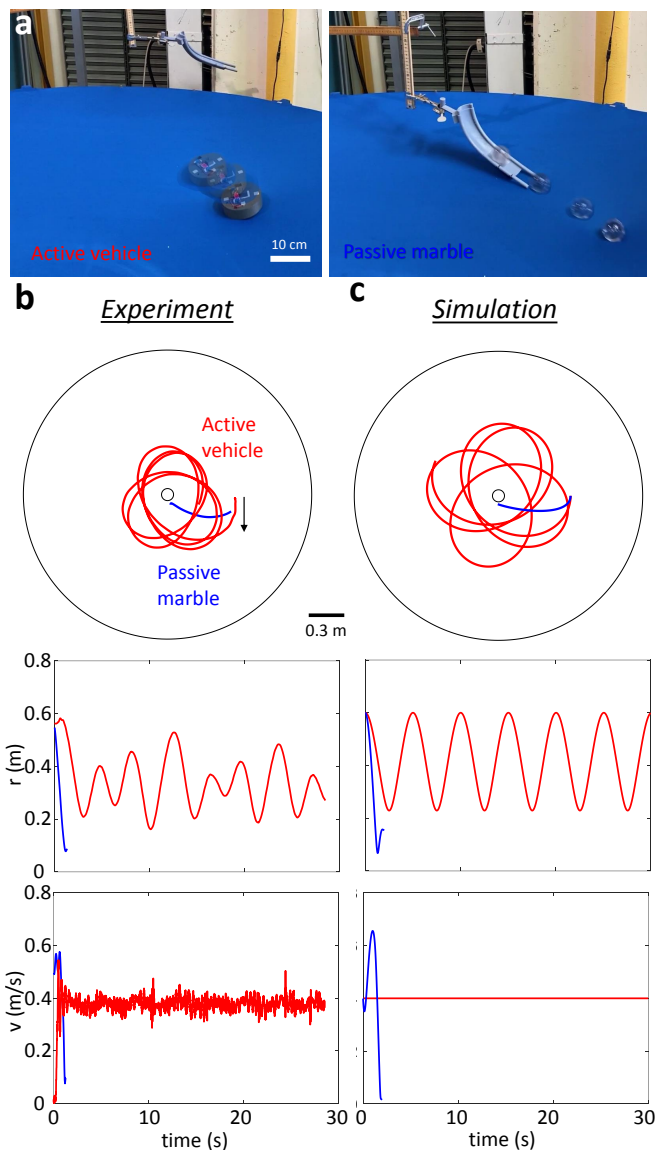


FIG. 2. Trajectories of passive and active objects on an elastic membrane. (a) Sample perspective views of an active vehicle and a passive marble moving on a Spandex membrane. The time interval between two consecutive snapshots is 0.17 s. (b) The experimental trajectories, radius evolution, and speed evolution of the active (red) and the passive (blue) objects with the same mass (150 g) on the same membrane started from the same initial position and velocity on the same membrane. (c) The simulation counterparts of (b).

be mirror reflections with each other. A first-order approximation with this symmetry could be $a \propto k(r) \sin \theta$ where the $k(r)$ is the radial dependence due to the local slope $\gamma(r)$ that changes with radius. One could imagine k increases with the local slope γ . The detail relation between k and γ would depend on the mechanical structure of the active object, but one could always Taylor expand this dependence. For preliminary study, here we assume linear dependence $k = C\gamma$.

While an active object follows equations Eqs. 2, 3, a

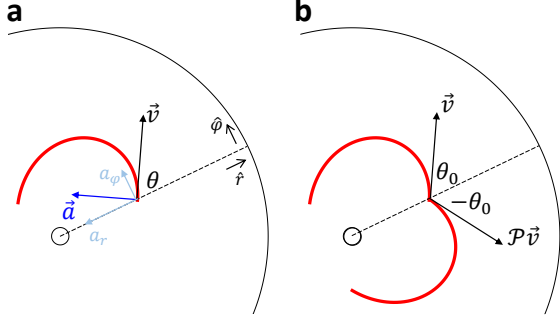


FIG. 3. **Dynamics of the active vehicle.** (a) The acceleration of an active vehicle is perpendicular to its velocity \vec{v} . (b) A non-chiral vehicle with a mirror-reflected initial velocity $\mathcal{P}\vec{v}$ will produce a mirror-reflected trajectory.

passive marble rolling on the membrane without slipping has a Lagrangian [8]

$$\mathcal{L} = \frac{7}{10}m \left((1 + z'(r)^2)\dot{r}^2 + r^2\dot{\varphi}^2 \right) - mgz(r). \quad (4)$$

If we consider the dissipation function to be an effective Coulomb rolling friction $D = -fv$ (See Sec. A of the Appendix) where $v = \sqrt{\dot{r}^2 + r^2\dot{\varphi}^2}$ and $f = \mu mg$, we arrive at a more realistic model by plugging the dissipation into the right hand side of the Euler-Lagrange equation $\frac{d}{dt} \left(\frac{\partial \mathcal{L}}{\partial \dot{q}} \right) - \frac{\partial \mathcal{L}}{\partial q} = -\frac{\partial D}{\partial \dot{q}}$ where q are r and φ .

$$(1 + z'^2)\ddot{r} + z'z''\dot{r}^2 - r\dot{\varphi}^2 + \frac{5}{7}gz' = -\frac{5}{7}\mu g \frac{\dot{r}}{v} \quad (5)$$

$$r^2\ddot{\varphi} + 2r\dot{r}\dot{\varphi} = -\frac{5}{7}\mu g \frac{r^2\dot{\varphi}}{v} \quad (6)$$

The left hand sides of the above equations are the same as the dynamical equations in [1] while the right hand sides correspond to the friction force.

Integration of the above models for the active vehicle and passive marble (Fig.2c) shows qualitative agreement with the experiments. Fig.2c shows the integration of the active dynamics Eqs. 2, 3 and the passive dynamics Eqs. 5, 6 on the same membrane measured from an experiment when the object started from the same position and velocity. The physical parameters are measured from experiments. The acceleration dependence on radius k for the active vehicle uses $k = C\gamma = C\partial_r z$ where $z(r)$ is measured from the height of the static vehicle placed at different radii r . The proportionality C uses the ratio between acceleration and the gradient $\partial_r z$ at the radius close to the edge of the elastic membrane. We probe the friction coefficient for the passive marble by measuring the dissipation of mechanical energy in a designed experiment (see Sec. A of the appendix).

The spacetime of the orbits. To functionally understand the feature of the orbit of the active object so that we are able to program it, the spacetime of these orbits

could provide us with insights. If we recognize similarity between the resultant spacetime metric and some known metrics, then we could understand how the orbital features depend on the system parameters.

In principle, the orbital dynamics we wish to map could be described by a diversity of metrics. But for simplicity, and to make the analogy with GR in the weak field limit, given the axi-symmetry of the system, we propose a metric of the form

$$ds^2 = -\alpha^2 dt^2 + \Phi^2(\Psi^2 dr^2 + r^2 d\varphi^2) \quad (7)$$

with $\alpha = \alpha(r)$, $\Phi = \Phi(r)$, $\Psi^2 = 1 + z'^2$. Here, the elements of the metric $g_{\alpha\beta}$ are zero except $g_{tt} = -\alpha^2$, $g_{rr} = \Phi^2\Psi^2$ and $g_{\varphi\varphi} = \Phi^2r^2$. Plug the $g_{\alpha\beta}$ into the Christoffel symbols $\Gamma_{\alpha\beta}^\mu$ in the geodesic equations $\ddot{x}^\mu + \Gamma_{\alpha\beta}^\mu \dot{x}^\alpha \dot{x}^\beta = 0$, we arrive at

$$\ddot{t} + \frac{(\alpha^2)'}{\alpha^2} \dot{t}\dot{r} = \frac{1}{\alpha^2} (\alpha^2 \dot{t})^\circ = 0 \quad (8)$$

$$\ddot{\varphi} + \frac{(\Phi^2 r^2)'}{\Phi^2 r^2} \dot{\varphi}\dot{r} = \frac{1}{\Phi^2 r^2} (\Phi^2 r^2 \dot{\varphi})^\circ = 0 \quad (9)$$

$$\ddot{r} + \frac{(\alpha^2)'}{2\Phi^2\Psi^2} \dot{t}^2 + \frac{(\Phi^2\Psi^2)'}{2\Phi^2\Psi^2} \dot{r}^2 - \frac{(\Phi^2 r^2)'}{2\Phi^2\Psi^2} \dot{\varphi}^2 = 0 \quad (10)$$

with λ as an affine parameter and $\dot{q} = dq/d\lambda$, $\ddot{q} = d^2q/d\lambda^2$. From Eqs. 8,9, we have that

$$\alpha^2 \dot{t} = E = \text{constant}, \quad (11)$$

$$\Phi^2 r^2 \dot{\varphi} = L = \text{constant}, \quad (12)$$

both a consequence that conservation of energy and angular momentum holds.

With the help of $\dot{q} = (dq/dt)(dt/d\lambda) = \dot{t}\dot{q}$ (see Sec. B of the appendix for details), the geodesic equations can be rewritten as

$$\ddot{\varphi} + \frac{2\dot{r}\dot{\varphi}}{r} = \left[\frac{(\alpha^2)'}{\alpha^2} - \frac{(\Phi^2)'}{\Phi^2} \right] \dot{r}\dot{\varphi} \quad (13)$$

$$\ddot{r} - \frac{r\dot{\varphi}^2}{\Psi^2} + \frac{\Psi'}{\Psi} \dot{r}^2 = \left[\frac{(\alpha^2)'}{\alpha^2} - \frac{(\Phi^2)'}{\Phi^2} \right] \dot{r}^2 + \frac{1}{2\Phi^2\Psi^2} [(\Phi^2)'\dot{v}^2 - (\alpha^2)'] \quad (14)$$

where primes denoting differentiation with respect to r .

Notice that the left hand side of Eqs. 13,14 are the components of the acceleration, a_φ and a_r respectively, in Eqs. 2,3. When we plug $\cos \theta = \dot{r}/v$, $\sin \theta = r\dot{\varphi}/v$ and $a = k \sin \theta$ into Eqs. 2,3, we have

$$\ddot{\varphi} + \frac{2\dot{r}\dot{\varphi}}{r} = \frac{k}{v^2} \dot{r}\dot{\varphi} \quad (15)$$

$$\ddot{r} - \frac{r\dot{\varphi}^2}{\Psi^2} + \frac{\Psi'}{\Psi} \dot{r}^2 = -\frac{k}{\Psi} \frac{r^2\dot{\varphi}^2}{v^2}. \quad (16)$$

Thus, comparing the right hand sides of Eqs. 13,14 and Eqs. 2,3 and noticing $\dot{r}^2 + r^2\dot{\varphi}^2 = v^2$ in Eq. 16 yield

the following relationships between the metric functions α and Φ in terms of the speed of the vehicle and k .

$$\frac{(\alpha^2)'}{\alpha^2} = \frac{k\Psi}{v^2} \left[\frac{\Phi^2 v^2}{\alpha^2 - \Phi^2 v^2} \right] \quad (17)$$

$$\frac{(\Phi^2)'}{\Phi^2} = \frac{k\Psi}{v^2} \left[\frac{2\Phi^2 v^2 - \alpha^2}{\alpha^2 - \Phi^2 v^2} \right]. \quad (18)$$

Integration of the above equations yields

$$\alpha^2 = -\frac{1}{C_1 v^2} + C_2 \cdot e^{-K/v^2} \quad (19)$$

$$\Phi^2 = \frac{\alpha^2}{v^2} + C_1 (\alpha^2)^2 \quad (20)$$

where $K = K(r) \equiv \int_0^r k(s)\Psi(s)ds$.

To determine the constants, we make use of the normalization condition and the fact that the metric should be flat at $k \rightarrow 0$.

The metric (Eq. 7) gives us normalization condition $-1 = -\alpha^2 \dot{t}^2 + \Phi^2 (\Psi^2 \dot{r}^2 + r^2 \dot{\varphi}^2)$. To exploit this condition, we want to eliminate the $d/d\lambda$ in \dot{r} like Eqs. 11, 12. Using $\dot{q} = (dq/dt)(dt/d\lambda) = \dot{t}\dot{q}$, Eqs. 11, 12, and the fact that $v^2 = r^2 \dot{\varphi}^2 + \dot{r}^2$, we have

$$\begin{aligned} \dot{r}^2 &= \left(\frac{E}{\alpha^2} \dot{r} \right)^2 \\ &= \frac{E^2}{(\alpha^2)^2} \frac{1}{\Psi^2} (v^2 - r^2 \dot{\varphi}^2) \\ &= \frac{E^2}{(\alpha^2)^2} \frac{1}{\Psi^2} \left[v^2 - r^2 \left(\frac{\alpha^2}{E} \dot{\varphi} \right)^2 \right] \\ &= \frac{E^2}{(\alpha^2)^2} \frac{1}{\Psi^2} \left[v^2 - r^2 \left(\frac{\alpha^2}{E} \frac{L}{\Phi^2 r^2} \right)^2 \right]. \end{aligned} \quad (21)$$

Plug the \dot{t} , \dot{r} , $\dot{\varphi}$ derived above into the normalization condition, we now have

$$-1 = -\frac{E^2}{\alpha^2} + \frac{\Phi^2 E^2 v^2}{(\alpha^2)^2}. \quad (22)$$

Plug in the α^2 and Φ^2 derived earlier (Eqs. 19,20), we have

$$-\frac{1}{E^2} = C_1 v^2. \quad (23)$$

Therefore $C_1 = -\frac{1}{v^2 E^2}$.

Another condition to determine the constants is that when $k = 0$, the metric is flat. In fact, $k(r) = 0$ indicates $K(r) = \int_{s=0}^r k(s)\Psi(s)ds = 0$. We set the lower limit of the integral to zero, without loss of generality, since otherwise the arbitrary constant will be absorbed by C_2 . This limit reduces the metric to

$$\begin{aligned} \alpha_0^2 &= -\frac{1}{C_1 v^2} + C_2 \\ \Phi_0^2 &= \frac{\alpha_0^2}{v^2} + C_1 (\alpha_0^2)^2 \end{aligned}$$

where $\alpha_0 \equiv \lim_{k \rightarrow 0} \alpha$ and $\Phi_0 \equiv \lim_{k \rightarrow 0} \Phi$.

To satisfy the flatness that $\alpha_0 = \Phi_0$, we need

$$\begin{aligned} \alpha_0^2 &= \frac{\alpha_0^2}{v^2} + C_1 (\alpha_0^2)^2 \\ 1 &= \frac{1}{v^2} + C_1 \left(-\frac{1}{C_1 v^2} + C_2 \right) \\ C_1 C_2 &= 1. \end{aligned} \quad (24)$$

Plug the conditions Eqs. 23,24 into the metric with undetermined coefficients Eqs. 19,20, we finally arrive at

$$\alpha^2 = E^2 (1 - v^2 e^{-K/v^2}) \quad (25)$$

$$\Phi^2 = E^2 e^{-K/v^2} (1 - v^2 e^{-K/v^2}). \quad (26)$$

The quantity E is a constant of motion (energy) associated with the fact that the metric is time-independent. The other constant of motion is L (angular momentum) associated with the metric's φ -symmetry.

Thus our formulation indeed reveals that the vehicle does not simply follow spatial geodesics of the membrane but instead follows geodesics in an emergent spacetime generated by the global curvature, the local curvature, the active dynamics, and the differential mechanism. The resultant dynamics can now be understood as those of a test particle in a new spacetime where the active feature of the real particle, such as a persistently controlled speed, generates a non-splittable effective spacetime for the test particle (i.e. g_{tt} is not constant). In the language of the work by Price [9], the effects of curvature are now not restricted to space [10]. That is, in general, the metric function g_{tt} could depend on both the coordinate time (t) as well as the spatial coordinates. For a static metric (i.e., the metric functions are independent of time), the spacetime becomes splittable when g_{tt} does not depend on the spatial coordinates. This leads to only spatial curvature. It was argued in [9] that the spatial curvature is different from the spacetime curvature as it is devoid of gravity, i.e., a free particle initially at rest will remain at rest.

The essential contribution from active drive is the persistent response to the local curvature, here particularly enabled by the controlled constant speed unseen in passive systems. In fact, when the response of the turning to the local slope vanishes at the limit $v \rightarrow \infty$ such that $\alpha^2 = \Phi^2 = E^2(1 - v^2)$, the metric Eq. 7 with components Eqs. 25,26 reduces to a splittable (and flat) spacetime Eq. 1. On the other hand, when v is finite and controllable, the active locomotion provides more flexibility and programmability in fabricating the desired spacetime depicted by GR than the passive agents studied in the previous works such as the dissipative marbles [1, 8] rolling on a membrane. For instance, the conserved quantity directly led from the metric could show that a k increasing with r makes an orbit have a precession with a sign opposite to the orbit while a k decreasing with r makes an orbit have a precession with

a sign same as the orbit [6].

Programming arbitrary spacetime with speed-varying active object. The metric Eqs. 25,26 has shown us how the parameters of the system change the spacetime and thus the orbit. Now we want to see how we can do the inverse problem to program the desired spacetime with the system parameters (e.g., $k(r)$ and $v(r)$).

In metric Eqs. 25,26, we can tune the speed and membrane elasticity to change the spacetime of the orbits. However, here the spatial and radial metric are not completely disentangled yet. To have two degrees of freedom such that we can indeed program the spacetime arbitrarily, one could introduce another degree of freedom. For instance, if we allow the speed v to vary with the radius r (physical instantiation could be achieved by inferring the radius from the instantaneous tilting angle γ), Eqs. 17, 18 with $\Psi^2 \approx 1$ give the requirement of mapping as

$$\frac{(\alpha^2)'}{\alpha^2} - \frac{(\Phi^2)'}{\Phi^2} = \frac{v'}{v} + \frac{k}{v^2} \quad (27)$$

$$\frac{(\Phi^2)'v^2 - (\alpha^2)'}{2\Phi^2} = -k. \quad (28)$$

These two equations above give us the recipe to create desired spacetime by changing the speed of the vehicle with radius. For a desired metric with spatial curvature $\Phi^2(r)$ and temporal curvature $\alpha^2(r)$, we can solve for the required membrane elasticity and object speed by plugging in the curvatures into these two equations. The solution (see Sec. C of the appendix for details) is

$$v(r)^2 = \left(\int_{r_1}^r f(r') \cdot \frac{(\alpha^2)'(r')}{\Phi^2(r')} dr' \right) / f(r) \quad (29)$$

where

$$f(r) = -e^{\int_{r_1}^r -2\frac{(\alpha^2)'(r')}{\alpha^2(r')} + \frac{(\Phi^2)'(r')}{\Phi^2(r')} dr'}. \quad (30)$$

For instance, if we plug in the Schwarzschild metric in isotropic coordinates $\alpha^2(r) = 1 - r_s/r$, $\Phi^2(r) = (1 - r_s/r)^{-1}$, we arrive at the prescription for the membrane elasticity $k(r)$ and active object speed $v(r)$ as shown in Fig.4a. Analytically,

$$v(r)^2 = r_s \frac{(r - r_s)^2}{r^3} + C \left(\frac{r - r_s}{r} \right)^3 \quad (31)$$

$$k(r) = \frac{r_s(r - r_s)(r + Cr + r_s - Cr_s)}{2r^4} \quad (32)$$

where

$$C = \frac{v_0^2 r_0^3}{(r_0 - r_s)^3} - \frac{r_s}{r_0 - r_s}. \quad (33)$$

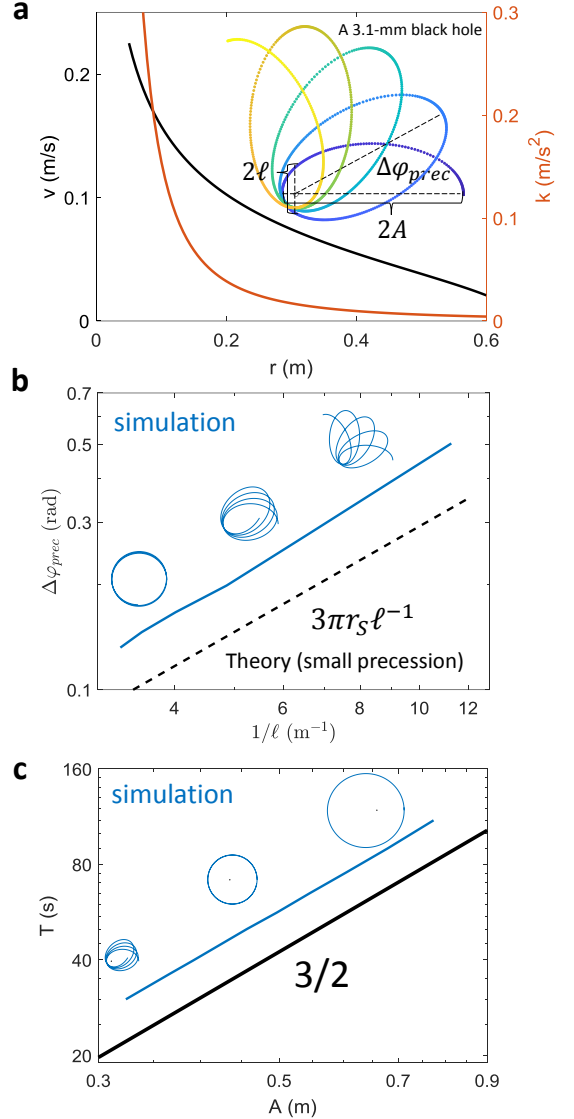


FIG. 4. Creating Schwarzschild orbit with speed varying particle. (a) The speed and membrane elasticity's dependence on radius to create an Schwarzschild black hole with $r_s = 3.1$ mm. The inset shows a precessing orbit with $A = 0.3$ m by using this prescription. (b) Precession angle $|\Delta\varphi_{prec}|$ as a function of inverse latus rectum. (c) The relation between the orbital period T and the semi major-axis A follows the Kepler's law as $T \propto A^{3/2}$. Insets in (b) and (c) show the trajectories around the data points.

Here, v_0 is the vehicle speed at r_0 as the boundary condition. One can use the inner radius as r_0 for instance.

Simulations using this prescription show features of Schwarzschild orbit such as the linear dependence of precession angle in terms of the inverse latus rectum. For Schwarzschild orbits with small precession, the precession angle increases with the inverse latus rectum as $\Delta\varphi_{prec} = 6\pi G^2 M / (c^2 l) = 3\pi r_s \ell^{-1}$ where G is the gravitational constant, M is the mass of the star, c is the

speed of light, and $\ell \equiv A(1 - e^2)$ is the latus rectum. We evaluate the semi major-axis A and the eccentricity e using the minimum and maximum radii: $A = (r_{\max} + r_{\min})/2$, $e = (r_{\max} - r_{\min})/(r_{\max} + r_{\min})$. Fig. 4b shows the precession angle $\Delta\varphi_{\text{prec}}$ as function of the inverse of the latus rectum ℓ^{-1} from simulations given $v_0 = v(r_0 = 0.05\text{m}) = 0.225$ m/s and $r_s = 0.0031$ m. The curve qualitatively follows the linear relationship, with small deviation from the theory due to the large precession angle. By changing (r_0, v_0) , we can get larger angular momenta and thus larger orbits around the same blackhole. These orbits show a relation between period T and semi major-axis A following the Kepler's law (Fig.4c).

To achieve this in experiments, a vehicle must actively vary its speed with radius and a membrane must have a radial dependence of its elastic modulus. One possible solution for the vehicle is to attach a tilt sensor to infer the radius and change the speed. To program the membrane with radially varying profile $k(r) = Cg|\partial_r z|$, here we consider a membrane with linear elasticity following the Poisson Equation $\nabla \cdot E\nabla z = P$ where P is the unit load from the membrane gravity. One possible way is to obtain the desired $k(r)$ is to create an elastic material with a radially varying thickness $P = P(r)$. Another option is to fabricate a membrane with a radially varying modulus $E = E(r)$.

Discussion. In this paper, we demonstrated how the use of an active particle –a robot – moving on an elastic membrane can generate a system which can mimic dynamics of bodies in arbitrary spacetime. Given the flexibility in construction and programming vehicles, our system makes for an attractive target to push toward a mechanical analog GR system; while superficially our system resembles the educational tool used to motivate Einstein's view of spacetime curvature influencing matter trajectories [1, 3, 8], unlike such systems which are *not* good analogs of GR, the activity allows the dynamics of the vehicle to be dictated by the curvature of "spacetime", not just the curvature of space as in splittable spacetimes (g_{tt} is constant) [9]. Thus we posit that mechanical analog "robophysical" [4, 11] systems can complement existing fluid [12, 13], condensed matter [14], atomic, and optical [15–17] analog gravity systems [18] given the ability to create infinite types of spacetimes. Further, we might even generate analogies to wave-like systems [19–21]; for example, one could increase the speed of the vehicle to be comparable to disturbance propagation (such that the membrane would follow the wave equation).

Beyond its role as a mechanical analog for GR, this framework could also provide a new perspective to understand active matter undergoing field-mediated interactions [6, 22]. For instance, the spacetime metric of the agents' motion can both guide our choice of parameter

values to alter orbital features like the precession sign and influence our design of control schemes that accomplish tasks like helping multiple agents avoid mergers on the membrane [6].

ACKNOWLEDGMENTS

We thank Lutian Zhao for the help on differential equation. Funding for D.I.G. and S.L. provided by ARO and ARL MAST CTA; funding also provided by Dunn Family Professorship. P.L. supported by NSF Grants 1908042 1806580 1550461. G.L. supported by NASA Grants 80NSSC20K0641 and 80NSSC20K0522

-
- [1] C. A. Middleton and D. Weller, *American Journal of Physics* **84**, 284 (2016).
 - [2] G. D. White, *American Journal of Physics* **81**, 890 (2013).
 - [3] G. D. White and M. Walker, *American Journal of Physics* **70**, 48 (2002).
 - [4] J. Aguilar, T. Zhang, F. Qian, M. Kingsbury, B. McInroe, N. Mazouchova, C. Li, R. Maladen, C. Gong, M. Travers, *et al.*, *Reports on Progress in Physics* **79**, 110001 (2016).
 - [5] Y. O. Aydin, J. M. Rieser, C. M. Hubicki, W. Savoie, and D. I. Goldman, in *Robotic Systems and Autonomous Platforms* (Elsevier, 2019) pp. 109–127.
 - [6] S. Li, Y. Ozkan Aydin, C. Xiao, G. Small, H. N. Gynai, G. Li, J. M. Rieser, P. Laguna, and D. I. Goldman, arXiv preprint arXiv:2004.03549 (2021).
 - [7] J. A. Wheeler and K. W. Ford, *Geons, Black Holes, and Quantum Foam* (Norton & Company, 2000).
 - [8] C. A. Middleton and M. Langston, *American Journal of Physics* **82**, 287 (2014).
 - [9] R. H. Price, *American Journal of Physics* **84**, 588 (2016).
 - [10] P. Batlle, A. Teixidó, J. Llobera, I. Medrano, and L. C. Pardo, *European Journal of Physics* **40**, 045005 (2019).
 - [11] Y. O. Aydin, J. M. Rieser, C. M. Hubicki, W. Savoie, and D. I. Goldman, in *Robotic Systems and Autonomous Platforms*, Woodhead Publishing in Materials, edited by S. M. Walsh and M. S. Strano (Woodhead Publishing, 2019) pp. 109–127.
 - [12] W. G. Unruh, *Physical Review Letters* **46**, 1351 (1981).
 - [13] S. Patrick, A. Coutant, M. Richartz, and S. Weinfurter, *Physical review letters* **121**, 061101 (2018).
 - [14] J. Steinhauer, *Nature Physics* **12**, 959 (2016).
 - [15] J. Zhu, Y. Liu, Z. Liang, T. Chen, and J. Li, *Physical review letters* **121**, 234301 (2018).
 - [16] T. G. Philbin, C. Kuklewicz, S. Robertson, S. Hill, F. König, and U. Leonhardt, *Science* **319**, 1367 (2008).
 - [17] F. Belgiorno, S. L. Cacciatori, M. Clerici, V. Gorini, G. Ortenzi, L. Rizzi, E. Rubino, V. G. Sala, and D. Facio, *Physical review letters* **105**, 203901 (2010).
 - [18] C. Barceló, S. Liberati, and M. Visser, *Living Reviews in Relativity* **14**, 3 (2011).
 - [19] Y. Couder, S. Protiere, E. Fort, and A. Boudaoud, *Nature* **437**, 208 (2005).
 - [20] J. W. Bush, *Annual Review of Fluid Mechanics* **47**, 269 (2015).

- [21] J. W. M. Bush, Proceedings of the National Academy of Sciences **107**, 17455 (2010), <https://www.pnas.org/content/107/41/17455.full.pdf>.
- [22] G. Wang, T. V. Phan, S. Li, M. Wombacher, J. Qu, Y. Peng, G. Chen, D. I. Goldman, S. A. Levin, R. H. Austin, *et al.*, Physical review letters **126**, 108002 (2021).

Appendix

A. Probing the effective friction

Although the rolling friction can be complicated and the dissipation into the membrane could make it even more complicated, we probe the magnitude of an effective friction that absorbs all dissipative forces by doing the following experiment. We release the marble at the rim of the circular membrane with zero speed and thus zero kinetic energy. The marble then rolls radially towards the center, passes through the center, and stops before it reaches the other end of the diameter due to the effective rolling friction. Absorbing the loss of mechanical energy into the dissipation from the effective rolling friction f_{roll} for a distance of ℓ , we arrive at

$$f_{\text{roll}}\ell = mg\Delta h \quad (34)$$

The measurements from experiment that $\ell = 1.5$ m, $\Delta h = 0.1$ m give the effective friction coefficient $\mu = f_{\text{roll}}/mg = \Delta h/\ell = 0.07 \sim 0.1$.

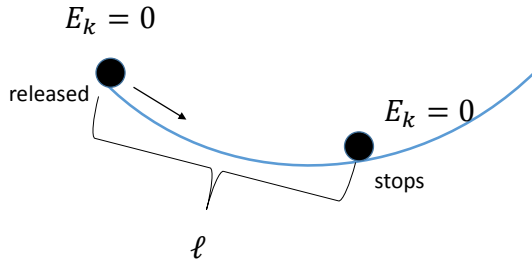


FIG. 5. An experiment to probe the effective friction.

B. Converting derivatives

With the help of $\dot{q} \equiv \frac{dq}{d\lambda} = \frac{dt}{d\lambda} \frac{dq}{dt}$ and $\alpha^2 \dot{t} = E$, $\Phi^2 r^2 \dot{\varphi} = L$ in Eqs. 11,12, we have

$$\dot{t} = \frac{E}{\alpha^2} \quad (35)$$

$$\begin{aligned} \ddot{t} &= \frac{dt}{d\lambda} \frac{d\dot{t}}{dt} \\ &= \frac{E}{\alpha^2} \frac{d}{dt} \left(\frac{E}{\alpha^2} \right) \\ &= -\frac{E^2 (\alpha^2)'}{(\alpha^2)^3} \dot{t} \end{aligned} \quad (36)$$

$$\dot{r} = \frac{dt}{d\lambda} \frac{dr}{dt} = \frac{E}{\alpha^2} \dot{r} \quad (37)$$

$$\begin{aligned} \ddot{r} &= \frac{dt}{d\lambda} \frac{d\dot{r}}{dt} \\ &= \frac{E}{\alpha^2} \cdot \frac{d}{dt} \left(\frac{E}{\alpha^2} \dot{r} \right) \\ &= \frac{E^2}{(\alpha^2)^2} \cdot \left(-\frac{(\alpha^2)'}{\alpha^2} \dot{r}^2 + \ddot{r} \right) \end{aligned} \quad (38)$$

$$\dot{\varphi} = \frac{dt}{d\lambda} \frac{d\varphi}{dt} = \frac{E}{\alpha^2} \dot{\varphi} \quad (39)$$

$$\begin{aligned} \ddot{\varphi} &= \frac{dt}{d\lambda} \frac{d\dot{\varphi}}{dt} \\ &= \frac{E}{\alpha^2} \frac{d}{dt} \left(\frac{E}{\alpha^2} \dot{\varphi} \right) \\ &= \frac{E^2}{(\alpha^2)^2} \cdot \left(-\frac{(\alpha^2)'}{\alpha^2} \dot{r} \dot{\varphi} + \ddot{\varphi} \right). \end{aligned} \quad (40)$$

C. Programming the metric

By eliminating the k in Eqs. 27,28, we get

$$MV - V' = \frac{(\alpha^2)'}{\Phi^2} \quad (41)$$

where $M(r) = 2(\alpha^2)'(r)/\alpha^2(r) - (\Phi^2)'(r)/\Phi^2(r)$ and $V(r) = v^2(r)$.

We can multiply a function $f(r)$ to both sides of Eq. 41 to make the left hand side exact. Noting $(fV)' = f'V + fV'$, we need $f'/f = -M$. Therefore,

$$f(r) = -e^{\int_{r_1}^r -M(r') dr'}. \quad (42)$$

With this f , we now have $(fV)' = f(\alpha^2)'/\Phi^2$. So,

$$V(r) = \left(\int_{r_1}^r f(r') \cdot \frac{(\alpha^2)'(r')}{\Phi^2(r')} dr' \right) \cdot \frac{1}{f(r)}. \quad (43)$$

By plugging in the Schwarzschild metric in isotropic coordinates $\alpha^2(r) = 1 - r_s/r$, $\Phi^2(r) = (1 - r_s/r)^{-1}$, we have

$$\begin{aligned} f(r) &= -e^{\int_{r_1}^r -\frac{3r_s}{r'(r'-r_s)} dr'} \\ &= -e^{(C_1 + 3 \log(r/(r-r_s)))} \\ &= -C_2 \cdot \left(\frac{r}{r-r_s} \right)^3. \end{aligned} \quad (44)$$

Therefore,

$$\begin{aligned}
V(r) &= \left(\int_{r_1}^r C_2 \cdot \left(\frac{r'}{r' - r_s} \right)^3 \cdot \frac{(r' - r_s)r_s}{r'^3} dr' \right) / f(r) \\
&= \left(\int_{r_1}^r C_2 \cdot \frac{r_s}{(r' - r_s)^2} dr' \right) / f(r) \\
&= (-C_2 \frac{r_s}{r - r_s} + C_3) / (-C_2 \cdot \left(\frac{r}{r - r_s} \right)^3) \\
&= r_s \frac{(r - r_s)^2}{r^3} + C \left(\frac{r - r_s}{r} \right)^3 \tag{45}
\end{aligned}$$

$$\begin{aligned}
k(r) &= -\frac{(\Phi^2)'V - (\alpha^2)'}{2\Phi^2} \\
&= \frac{(r - r_s)r_s(r + Cr + r_s - Cr_s)}{2r^4}. \tag{46}
\end{aligned}$$

To program the active object physically, we want to prescribe the speed v_0 at a certain radius (say the inner

radius r_0) so that $V(r_0) = v_0^2$, we need

$$C = \frac{v_0^2 r_0^3}{(r_0 - r_s)^3} - \frac{r_s}{r_0 - r_s}. \tag{47}$$

Further, a reasonable speed v_c at a characteristic orbit size (say the circular orbit r_c) will limit the size of the Schwarzschild radius r_s (the size of the black hole) with $\frac{V(r_c; r_s)}{r_c} = k(r_c)$.

Contributions

S.L. and P.L. designed the theoretical model; S.L., P.L. and G.L. contributed to theory and the numerical simulations; S.L., H.G. and S.T. performed the experiments; S.L., P.L. and D.I.G. designed the research and wrote the paper; D.I.G. guided overall research program.